Arch Appl Mech (2005) 74: 863–877
DOI 10.1007/s00419-005-0412-7

ORIGINAL

J. Schröder · H. Romanowski

A thermodynamically consistent mesoscopic model for transversely isotropic ferroelectric ceramics in a coordinate-invariant setting

Received: 26 January 2005 / Accepted: 27 May 2005 / Published online: 12 November 2005

Abstract In this contribution we present a phenomenological mesoscopic thermodynamically consistent model for the description of switching processes in ferroelectric materials that is able to describe the fundamental electromechanical hysteresis effects. The main goal is to develop a representation using the set of independent variables, the strains and the electric field, in a coordinate-invariant setting. This formulation is particularly suitable for the treatment of a variety of complex boundary-value problems (BVP) with regard to the essential boundary conditions. Here we restrict ourselves to transversely isotropic solids. The anisotropic behavior is governed by isotropic tensor functions that depend on a finite set of invariants. Thus the material symmetry requirements are automatically fulfilled.

Keywords Invariant theory · Ferroelectrics · Polarization · Butterfly hysteresis · Dielectric hysteresis

1 Introduction

The microscopic structure of ferroelectric materials has of a crystalline nature. Typical materials that exhibit useful electromechanical coupling effects, like the typical Perovskite-type ferroelectric ceramics $BaTiO_3$ or PZT, are not produced as ideal single crystals but as polycrystals. Polycrystalline materials consist of a large number of crystals (grains), these crystals being subdivided into domains separated by the domain walls. Each stable domain has an individual polarization direction. Therefore, on the macroscale we consider a polycrystal, on the mesoscale domains with equal polarization directions are taken into account, whereas the microscale is defined by the underlying unit cells of the ceramic. In the following discussion we will focus on single domains consisting of single crystals with equal polarizations, which constitutes our mesoscopic scale by definition. Thus, the polycrystalline behavior could be obtained via a homogenization procedure applied to the mesoscale, which is not the focus of this paper. The main characteristics of these materials, below the Curie temperature ϑ_C, are the appearance of the so-called dielectric hysteresis loops and the butterfly hysteresis loops under applied oscillating electric fields. On the mesoscopic level we observe a switching of the polarization vector due to electrical and mechanical loads; the electrical loading can induce a 180° or 90° (ferroelectricity) and a mechanical loading can induce a 90° domain switching (ferroelasticity). In the ferroelectric phase a relative displacement of the centers of gravity of the positive and negative charge carriers at the microscopic level gives rise to polarization. Thus the ferroelectric ceramics possess a so-called remanent polarization P^r even when no external electrical field is applied. In some materials there could exist a striking difference between the spontaneous P_s and the remanent polarization, see Fig. 1, in contrast to ideal perfect crystals (they would possess $P_s = P^r$) or materials with free dipoles (e.g., water). This difference is the outcome of defects such as dislocations and impurities.

J. Schröder (✉) · H. Romanowski
Institut für Mechanik, Fachbereich Bauwissenschaften, Universität Duisburg-Essen, 45117 Essen, Universitätsstr. 15, Germany.
Tel.: +49-201-1832708; Fax: +49-2011832680; E-mail: j.schroeder@uni-essen.de

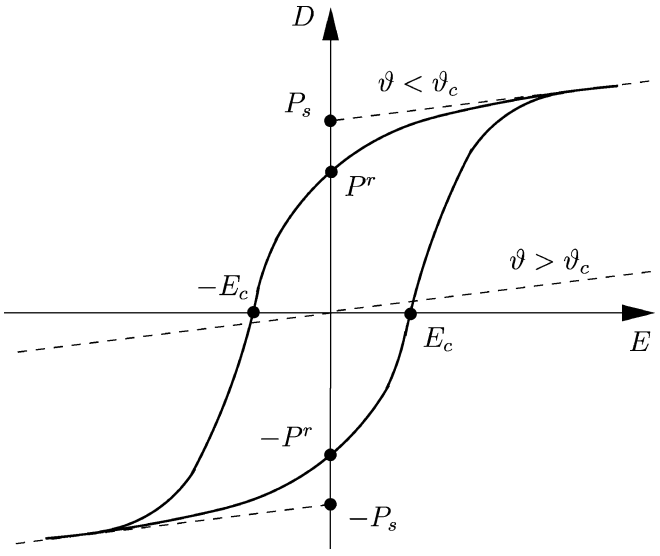

Fig. 1 Characteristic behavior in the ferroelectric phase $\vartheta < \vartheta_c$

In recent years a variety of microscopically and thermodynamically motivated constitutive models for the description of ferroelectric ceramics have been proposed in the literature. A general framework of the electrodynamics of continua within the scope of finite strains is presented in detail in [10] and [11]; in this context see also the extensive list of references therein. Chen and Tucker [8] proposed a one-dimensional (1D) model for the calculation of the typical hysteresis loop as a consequence of domain switching due to applied oscillating electric fields, neglecting cross-couplings between polar and lateral effects. The essential ingredient is a rate law for the effective number of aligned dipoles, depending on the external electric field (and the mechanical strains). In this context see also [7]. A framework for the development of phenomenological constitutive laws at the macroscopic scale is presented in [27]. Experimental results of polarization and depolarization of lead lanthanum zirconate titanate (PLZT) can be found, e.g., in [12]. The authors propose a heuristic hysteresis model, applicable for ferroelectric and ferroelastic switching, and perform a Reuss-type averaging technique in order to approximate the overall behavior of a polycrystalline specimen.

A three-dimensional (3D) switching model for the simulation of polycrystalline ferroelectric ceramics is proposed in [13]. In the latter works an energy-based switching criterion with combined electrical and mechanical contributions is used. An expansion of these works, suitable for finite-element calculations, is given in [14, 15]. A 1D phenomenological constitutive model for ferroelectric materials has been proposed in [17], which has been extended to a 3D model in [18]. A thermodynamically consistent formulation of the electromechanical hysteresis can be found in [1–4]. In these contributions concepts of phenomenological plasticity theory, including yield surfaces and isotropic and kinematic hardening based on the Helmholtz free energy, are used. Based on these concepts several approaches for thermodynamically motivated constitutive laws of ferroelectric ceramics have been developed.

A constitutive model based on microscopically motivated internal variables is proposed in [20], where depolarization effects have also been taken into account. A multiaxial thermodynamically consistent realization of the description of ferroelectric ceramics is presented in [21] (see also [9]), where the postulated switching surfaces and associated flow rules guarantee a positive dissipation during switching. A simplified formulation of this approach, which reduces the number of the internal variables, can be found in [28]. An overview concerning the development of the modeling of ferroelectrics can be found in [19]. Furthermore, the physical background, physical observations, and aspects of the complex behavior of ferroelectrics as well as the fatigue in such ceramics is reported in the review article [26]. It should be remarked that for some rate-independent ferroelectric models quite general conditions, which guarantee the existence of solutions, have recently been provided in [29].

In this contribution we describe the complex electromechanical behavior of ferroelectric materials with an oriented internal structure and with tensor-valued functions governed by basic and mixed invariants based on the concept of structural tensors. The advantage of such formulations is that general invariant forms of the constitutive equations lead to rational strategies for the modeling of the complex anisotropic response

functions. In addition, an efficient framework qualified for the implementation of arbitrary nonlinear response functions is obtained. Here we are mainly interested in the formulation of a mesoscopic model, where the orientations of the assumed transversely isotropic unit cells have to be taken into account. Therefore, we present a thermodynamically consistent model for transversely isotropic ferroelectric materials within the framework of the invariant theory, based on the coordinate-invariant formulations proposed in [31]. The invariant forms of the stress response function and the electric displacement function are derived from a scalar-valued free electromechanical enthalpy function. The proposed formulation can be applied to a variety of model problems for the simulation of the material behavior with irreversible (nonlinear) characteristics. These invariant forms satisfy the symmetry relationships of the considered body for the mechanical and electrical quantities a priori, i.e., they are automatically invariant under coordinate transformations of elements of the material symmetry group.

2 Governing equations of electromechanical BVP

2.1 Strong forms of electromechanical BVP

Let $\mathcal{B} \subset \mathbf{R}^3$ be the body of interest that is parameterized in $\boldsymbol{x}$. Furthermore, let $\boldsymbol{u}$ be the displacement field. The basic variables are the linear strain tensor, which is defined by the symmetric part of the displacement gradient, and the electric field vector $\boldsymbol{E}$, given by the negative gradient of the scalar potential ϕ:

$$\boldsymbol{\varepsilon}(\boldsymbol{x}) := \tfrac{1}{2}(\mathrm{grad}[\boldsymbol{u}] + \mathrm{grad}^T[\boldsymbol{u}]) \quad \text{and} \quad \boldsymbol{E}(\boldsymbol{x}) := -\mathrm{grad}[\phi] \; . \tag{1}$$

The governing field equations for the quasistatic case are the equation of equilibrium and the Gauss equation

$$\mathrm{div}[\boldsymbol{\sigma}] + \bar{\boldsymbol{f}} = \boldsymbol{0} \quad \text{and} \quad \mathrm{div}[\boldsymbol{D}] = \rho_f \; , \tag{2}$$

respectively. Here $\boldsymbol{\sigma}$ represents the symmetric Cauchy stress tensor, $\bar{\boldsymbol{f}}$ is the given body force, $\boldsymbol{D}$ is the vector of electric displacements, and ρ_f denotes the given density of free charge carriers. The surface of the body is decomposed into mechanical $\partial\mathcal{B} = \partial\mathcal{B}_u \bigcup \partial\mathcal{B}_\sigma$ and electrical parts $\partial\mathcal{B} = \partial\mathcal{B}_\phi \bigcup \partial\mathcal{B}_D$, with $\partial\mathcal{B}_u \bigcap \partial\mathcal{B}_\sigma = \emptyset$ and $\partial\mathcal{B}_\phi \bigcap \partial\mathcal{B}_D = \emptyset$. An illustration of this decomposition is depicted in Fig. 2a, b, where the vector $\boldsymbol{a}$ should suggest that there exists a preferred direction of the material due to its anisotropic behavior, see Sect. 3.1.

The boundary conditions for the displacements, the surface tractions $\bar{\boldsymbol{t}}$, the electric potential, and the electric surface charge $\bar{q}$ are defined by

$$\begin{array}{llll} \boldsymbol{u} = \bar{\boldsymbol{u}} & \text{on } \partial\mathcal{B}_u & \text{and} & \boldsymbol{t} = \bar{\boldsymbol{t}} = \boldsymbol{\sigma}\cdot\boldsymbol{n} \quad \text{on } \partial\mathcal{B}_\sigma \; , \\ \phi = \bar{\phi} & \text{on } \partial\mathcal{B}_\phi & \text{and} & -q = -\bar{q} = \boldsymbol{D}\cdot\boldsymbol{n} \quad \text{on } \partial\mathcal{B}_D \; , \end{array} \tag{3}$$

where $\boldsymbol{n}$ is a unit vector normal to the surface directed outward from the volume.

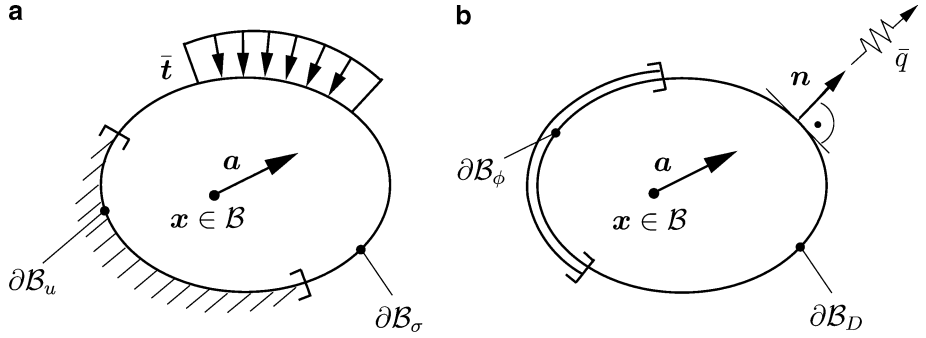

Fig. 2 Decomposition of the surface of the considered body $\partial\mathcal{B}$ into **a** mechanical $\partial\mathcal{B}_u \bigcup \partial\mathcal{B}_\sigma$ and **b** electrical $\partial\mathcal{B}_\phi \bigcup \partial\mathcal{B}_D$ parts

2.2 Weak forms of electromechanical BVP

In this section we summarize the basic steps for the derivation of the discrete weak forms needed for the numerical treatment of the coupled field equations within the Finite Element Method. This leads in the proposed framework to a symmetric formulation with no principal restrictions due to possible nonlinearities formulated in terms of the polynomial basis. The central field equations for electromechanical coupled solids are the balance of momentum $(2)_1$ and the Gauss law $(2)_2$. The boundary conditions for the displacements, the surface tractions, the electric potential, and the electric charge are defined in (3). A standard Galerkin procedure yields the weak forms of the governing field equations. The required test functions are denoted by $\delta\boldsymbol{u}$ and $\delta\phi$. They satisfy the homogeneous boundary conditions, i.e. $\delta\boldsymbol{u} = \boldsymbol{0}$ on $\partial\mathcal{B}_u$ and $\delta\phi = 0$ on $\partial\mathcal{B}_\phi$. Furthermore, we introduce the fields $\delta\boldsymbol{\varepsilon} := \frac{1}{2}(\mathrm{grad}[\delta\boldsymbol{u}] + \mathrm{grad}^T[\delta\boldsymbol{u}])$ and $\delta\boldsymbol{E} := \mathrm{grad}[\delta\phi]$. With these definitions we arrive at the weak forms

$$\begin{aligned} G_u &:= G_u^{int} - G_u^{ext} = 0 \quad \text{with} \quad G_u^{int} := \int_{\mathcal{B}} \delta\boldsymbol{\varepsilon} : \boldsymbol{\sigma}\, dv \,, \\ G_\phi &:= G_\phi^{int} - G_\phi^{ext} = 0 \quad \text{with} \quad G_\phi^{int} := \int_{\mathcal{B}} \delta\boldsymbol{E} \cdot \boldsymbol{D}\, dv \,. \end{aligned} \tag{4}$$

The external parts G_u^{ext} and G_ϕ^{ext} contain the given body force, the surface tractions, and the electric surface charge at the boundary, i.e.

$$G_u^{ext} := \int_{\partial\mathcal{B}_\sigma} \delta\boldsymbol{u} \cdot \bar{\boldsymbol{t}}\, da + \int_{\mathcal{B}} \delta\boldsymbol{u} \cdot \bar{\boldsymbol{f}}\, dv \quad \text{and} \quad G_\phi^{ext} := -\int_{\partial\mathcal{B}_D} \delta\phi\, \bar{q}\, da \,. \tag{5}$$

A spatial discretization of the body with n_{ele} finite elements, i.e. $\mathcal{B} \approx \bigcup_{e=1}^{n} \mathcal{B}^e$, leads to $G_u \approx \bigcup_{e=1}^{n} G_u^e$ and $G_\phi \approx \bigcup_{e=1}^{n} G_\phi^e$, where $G_{u,\phi}^e$ represents the weak forms of the associated balance laws for a typical finite element $\mathcal{B}^e$. A standard approximation of the actual and virtual displacement fields $\boldsymbol{u}^h = \boldsymbol{N}\boldsymbol{d}^e$ and $\delta\boldsymbol{u}^h = \boldsymbol{N}\delta\boldsymbol{d}^e$ yields

$$\boldsymbol{\varepsilon}^h := \boldsymbol{B}^e\boldsymbol{d}^e \quad \text{and} \quad \delta\boldsymbol{\varepsilon}^h := \boldsymbol{B}^e\delta\boldsymbol{d}^e \,, \tag{6}$$

where $\boldsymbol{N}$ denotes the matrix representation of the ansatz functions and $\{\boldsymbol{d}^e, \delta\boldsymbol{d}^e\}$ denote the actual and virtual node displacements of a typical element. Furthermore, for the individual electrical fields we obtain with $\boldsymbol{\phi}^h = \boldsymbol{N}\boldsymbol{\Phi}^e$ and $\delta\boldsymbol{\phi}^h = \boldsymbol{N}\delta\boldsymbol{\Phi}^e$ the expressions

$$\boldsymbol{E}^h := -\tilde{\boldsymbol{B}}^e\boldsymbol{\Phi}^e \quad \text{and} \quad \delta\boldsymbol{E}^h := \tilde{\boldsymbol{B}}^e\delta\boldsymbol{\Phi}^e \,, \tag{7}$$

where $\{\boldsymbol{\Phi}^e, \delta\boldsymbol{\Phi}^e\}$ denote the actual and virtual nodal electric potentials of an element. The matrices $\boldsymbol{B}^e$ and $\tilde{\boldsymbol{B}}^e$ contain the positive derivatives of the ansatz functions associated to the strains and the electric field, respectively. With the above approximation we obtain the discrete forms

$$\begin{aligned} G_u^{e,int,h} &:= \delta\boldsymbol{d}^{e,T} \int_{\mathcal{B}^e} \boldsymbol{B}^{e,T}\boldsymbol{\sigma}\, dv \,,\; G_u^{e,ext,h} := \delta\boldsymbol{d}^{e,T} \left[\int_{\partial\mathcal{B}_\sigma^e} \boldsymbol{N}^T\, \bar{\boldsymbol{t}}\, da + \int_{\mathcal{B}^e} \boldsymbol{N}^T\, \bar{\boldsymbol{f}} dv \right] , \\ G_\phi^{e,int,h} &:= \delta\boldsymbol{\Phi}^{e,T} \int_{\mathcal{B}^e} \tilde{\boldsymbol{B}}^{e,T}\boldsymbol{D}\, dv \,,\; G_\phi^{ext,h} := \delta\boldsymbol{\Phi}^{e,T} \int_{\partial\mathcal{B}_D^e} -\boldsymbol{N}^T\bar{q}\, da \,. \end{aligned} \tag{8}$$

For the solution of the discrete counterparts of the coupled, nonlinear weak forms we apply a Newton iteration scheme. This results in rather lengthy expressions that are not within the scope of this contribution. An alternative approach based on a vector-potential formulation of the electric displacements is given in [22].

3 Coordinate-invariant thermodynamic formulation

3.1 Concept of structural tensors

Let us now assume the existence of a thermodynamic potential that acts as an electric enthalpy function H. For the explicit formulation of coordinate-invariant constitutive equations the representations of isotropic tensor

functions are used. The governing equations have to represent the material (geometrical and physical) symmetries of the ceramic; the material symmetry group is denoted by $\mathcal{G}_{ti}$. Thus, the values of the enthalpy function have to be scalar invariants under all transformations $\boldsymbol{Q} \in \mathcal{G}_{ti}$ of the set of tensor variables involved in the scalar-valued function, i.e.,

$$\hat{H}(\boldsymbol{\varepsilon}, \boldsymbol{E}, \boldsymbol{\xi}) = \hat{H}(\boldsymbol{Q}\boldsymbol{\varepsilon}\boldsymbol{Q}^T, \boldsymbol{Q}\boldsymbol{E}, \boldsymbol{Q} * \boldsymbol{\xi}) \quad \forall \quad \boldsymbol{Q} \in \mathcal{G}_{ti} \,, \tag{9}$$

where $\boldsymbol{\xi}$ denotes the set of internal tensor-, vector-, and scalar-valued internal variables. The operator $(\boldsymbol{Q}*)$ characterizes the transformation of these variables. Let $\boldsymbol{T}$ be a tensor of second order, $\boldsymbol{v}$ a vector, and α a scalar; then we get $\boldsymbol{Q} * \boldsymbol{T} = \boldsymbol{Q}\boldsymbol{T}\boldsymbol{Q}^T$ and $\boldsymbol{Q} * \boldsymbol{v} = \boldsymbol{Q}\boldsymbol{v}$, as well as $\boldsymbol{Q} * \alpha = \alpha$, respectively. The transformation of higher-order tensorial quantities is self-explanatory. The invariance group $\mathcal{G}_{ti}$ of the electromechanically coupled solid can be obtained by the so-called *principle of the superposition of symmetries*, also known as the *Curie symmetry principle*, see Fig. 3. The principle states that the overall symmetry group of several objects is the highest common symmetry subgroup of these objects under consideration of the mutual orientations of their individual symmetry elements. It is given by

$$\mathcal{G}_{ti} = \{\boldsymbol{Q} \in \mathcal{O}(3), \quad \boldsymbol{Q}\boldsymbol{a} = \boldsymbol{a}\} \,, \tag{10}$$

see [24] and [31]. The main idea of the invariant theory is the extension of the $\mathcal{G}_{ti}$-invariant functions (9) to functions that are invariant under a larger group of transformations, particularly under all elements of the orthogonal group $\mathcal{O}(3)$. For the invariant formulation of the thermodynamic potential we introduce an additional tensor, the preferred direction $\boldsymbol{a}$, which can be interpreted as a first-order structural tensor. Using the so-called principle of isotropy of space, see e.g., [5], we get the representation

$$\hat{H}(\boldsymbol{\varepsilon}, \boldsymbol{E}, \boldsymbol{\xi}, \boldsymbol{a}) = \hat{H}(\boldsymbol{Q}\boldsymbol{\varepsilon}\boldsymbol{Q}^T, \boldsymbol{Q}\boldsymbol{E}, \boldsymbol{Q} * \boldsymbol{\xi}, \boldsymbol{Q}\boldsymbol{a}) \quad \forall \quad \boldsymbol{Q} \in \mathcal{O}(3) \,. \tag{11}$$

Equation (11) is the definition of an isotropic tensor function with respect to the whole set of tensorial arguments $\{\boldsymbol{\varepsilon}, \boldsymbol{E}, \boldsymbol{\xi}, \boldsymbol{a}\}$ and has to be interpreted as an anisotropic function with respect to the arguments $\{\boldsymbol{\varepsilon}, \boldsymbol{E}, \boldsymbol{\xi}\}$, i.e.

$$\hat{H}(\boldsymbol{\varepsilon}, \boldsymbol{E}, \boldsymbol{\xi}, \boldsymbol{a}) = \hat{H}(\boldsymbol{Q}\boldsymbol{\varepsilon}\boldsymbol{Q}^T, \boldsymbol{Q}\boldsymbol{E}, \boldsymbol{Q} * \boldsymbol{\xi}, \boldsymbol{a}) \quad \forall \quad \boldsymbol{Q} \in \mathcal{G}_{ti} \,. \tag{12}$$

The enthalpy function can be formulated in the basic and mixed invariants of the whole argument list because (11) is an isotropic tensor function. For the derivation of an integrity basis, the minimal number of independent invariants, we refer the reader to [5,24,34–37] and the references cited therein.

It should be noted that the relation between the symmetry of a crystal and the symmetry of its physical properties is established by *Neumann's principle*, i.e. the symmetry elements of any physical property of a crystal must include the symmetry elements of the point group of the crystal. As a consequence of the chosen material symmetry group, see (10), the polarization direction is fixed in our model and no ferroelasticity and mechanical depolarization can occur. Due to the chosen anisotropy class, which is characterized by only one preferred direction $\boldsymbol{a}$, the proposed mesoscopic model cannot describe the behavior of a polycrystal.

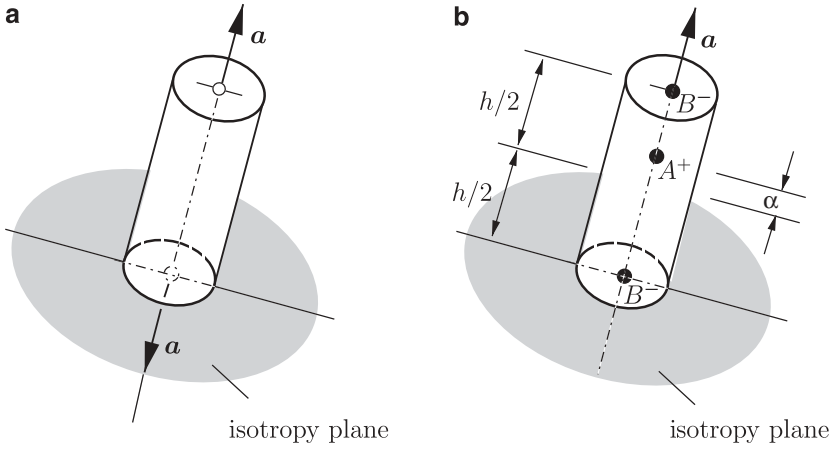

Fig. 3 Illustration of the principle of superposition of symmetries. **a** Invariance of the mechanical part with respect to $\pm\boldsymbol{a}$. **b** Polarization of the electrical part due to the distance between the centers of gravity of the positively and negatively charged particles within a unit cell constitutes invariance with respect to $+\boldsymbol{a}$

3.2 Additive decomposition of strains and electric displacements

One of the basic assumptions in the proposed model is the often-used additive decomposition of the strain tensor $\boldsymbol{\varepsilon}$ and the vector of electric displacements $\boldsymbol{D}$ into their reversible $\{\boldsymbol{\varepsilon}^e, \boldsymbol{D}^e\}$ and remanent parts $\{\boldsymbol{\varepsilon}^r, \boldsymbol{P}^r\}$:

$$\boldsymbol{\varepsilon} = \boldsymbol{\varepsilon}^e + \boldsymbol{\varepsilon}^r \quad \text{and} \quad \boldsymbol{D} = \boldsymbol{D}^e + \boldsymbol{P}^r \ . \tag{13}$$

Consequently, we choose for the set of internal variables in (11) the remanent quantities, i.e. $\boldsymbol{\xi} := \{\boldsymbol{\varepsilon}^r, \boldsymbol{P}^r\} \rightarrow \boldsymbol{Q} * \boldsymbol{\xi} = \{\boldsymbol{Q}\boldsymbol{\varepsilon}^r\boldsymbol{Q}^T, \boldsymbol{Q}\boldsymbol{P}^r\}$. The observable variables are the total strains $\boldsymbol{\varepsilon}$ and the electric field $\boldsymbol{E}$, whereas the remanent quantities describe the internal state of the material and $\boldsymbol{a}$ reflects the internal orientation of the polarized material. Disregarding thermal effects the second law of thermodynamics yields

$$\mathcal{D} = \boldsymbol{\sigma} : \dot{\boldsymbol{\varepsilon}} - \boldsymbol{D} \cdot \dot{\boldsymbol{E}} - \dot{H} \geq 0 \ . \tag{14}$$

The evaluation of the dissipation inequality leads to the expression

$$\mathcal{D} = (\boldsymbol{\sigma} - \partial_{\boldsymbol{\varepsilon}} H) : \dot{\boldsymbol{\varepsilon}} - (\boldsymbol{D} + \partial_{\boldsymbol{E}} H) \cdot \dot{\boldsymbol{E}} - \partial_{\boldsymbol{\varepsilon}^r} H : \dot{\boldsymbol{\varepsilon}}^r - \partial_{\boldsymbol{P}^r} H \cdot \dot{\boldsymbol{P}}^r \geq 0 \ . \tag{15}$$

This inequality has to be fulfilled for all possible thermodynamic processes; thus we obtain the following constitutive equations for the stresses and electric displacements:

$$\boldsymbol{\sigma} = \partial_{\boldsymbol{\varepsilon}} H \quad \text{and} \quad \boldsymbol{D} = -\partial_{\boldsymbol{E}} H \ , \tag{16}$$

respectively. For the thermodynamic forces associated to the remanent quantities we introduce the abbreviations

$$\tilde{\boldsymbol{\sigma}} := -\partial_{\boldsymbol{\varepsilon}^r} H \quad \text{and} \quad \tilde{\boldsymbol{E}} := -\partial_{\boldsymbol{P}^r} H \ , \tag{17}$$

which lead to the reduced dissipation inequality

$$\mathcal{D} = \tilde{\boldsymbol{\sigma}} : \dot{\boldsymbol{\varepsilon}}^r + \tilde{\boldsymbol{E}} \cdot \dot{\boldsymbol{P}}^r \geq 0 \ . \tag{18}$$

To describe the evolution of the remanent variables, the existence of a dissipation potential is assumed. This is expressed as a continuous, convex scalar-valued function of the flux variables $\dot{\boldsymbol{\varepsilon}}^r$ and $\dot{\boldsymbol{P}}^r$, in this context see e.g., [23,21,28]. Applying a Legendre–Fenchel transformation leads to a corresponding potential that can be formulated in terms of the dual quantities. Let us now introduce a switching surface Φ in terms of the dual variables $\tilde{\boldsymbol{\sigma}}$ and $\tilde{\boldsymbol{E}}$, with

$$\Phi(\tilde{\boldsymbol{\sigma}}, \tilde{\boldsymbol{E}}) \leq 0 \ . \tag{19}$$

Applying the principle of maximum remanent dissipation, a generalization of the principle of maximum dissipation, we construct the Lagrangian functional

$$\mathcal{L}(\tilde{\boldsymbol{\sigma}}, \tilde{\boldsymbol{E}}, \lambda) = -\mathcal{D}(\tilde{\boldsymbol{\sigma}}, \tilde{\boldsymbol{E}}) + \lambda \Phi(\tilde{\boldsymbol{\sigma}}, \tilde{\boldsymbol{E}}) \ , \tag{20}$$

with the Lagrange multiplier λ. The optimization conditions, see e.g., [25],

$$\partial_{\tilde{\boldsymbol{\sigma}}} \mathcal{L} = 0 \ , \quad \partial_{\tilde{\boldsymbol{E}}} \mathcal{L} = 0 \ , \quad \partial_{\lambda} \mathcal{L} = 0 \ , \tag{21}$$

lead to the associated flow rules of the remanent variables

$$\dot{\boldsymbol{\varepsilon}}^r = \lambda \partial_{\tilde{\boldsymbol{\sigma}}} \Phi(\tilde{\boldsymbol{\sigma}}, \tilde{\boldsymbol{E}}) \quad \text{and} \quad \dot{\boldsymbol{P}}^r = \lambda \partial_{\tilde{\boldsymbol{E}}} \Phi(\tilde{\boldsymbol{\sigma}}, \tilde{\boldsymbol{E}}) \tag{22}$$

and the loading/unloading conditions $\lambda \geq 0$, $\Phi(\tilde{\boldsymbol{\sigma}}, \tilde{\boldsymbol{E}}) \leq 0$, and $\lambda \Phi(\tilde{\boldsymbol{\sigma}}, \tilde{\boldsymbol{E}}) = 0$. It should be noted that the normality rule is sufficient to satisfy the second law of thermodynamics.

4 Model problem: transversely isotropic ferroelectric crystal

4.1 Polynomial basis

Hilbert's theorem postulates that, for a finite set of vectors and tensors, an integrity basis consisting of a finite number of invariants exists. In order to formulate the electric enthalpy function, we need this finite set of invariants, which builds the so-called polynomial basis. In the following discussion we are not interested in the derivation of the whole basis and refer the reader to [5] and [6] and references therein for an introduction to the invariant formulation of anisotropic constitutive equations and the representations for tensor functions. For detailed representations of scalar- and tensor-valued functions we refer to [36] and [37] and to the works [32,33]; see also [34,35]. In the context of electromechanical coupled systems see [31]. The finite set of vectors and tensors is given by the symmetric tensors $\boldsymbol{\varepsilon}$, $\boldsymbol{\varepsilon}^r$, the vectors $\boldsymbol{E}$, $\boldsymbol{P}^r$ and the preferred direction $\boldsymbol{a}$ with $||\boldsymbol{a}|| = 1$. With the normalization condition for $\boldsymbol{a}$, which induces $\text{trace}[(\boldsymbol{a} \otimes \boldsymbol{a})^n] = 1$ for $n = 1, 2, 3$, the basic and mixed invariants of interest in the proposed model are

$$\begin{gathered} I_1 := \text{trace}[\boldsymbol{\varepsilon} - \boldsymbol{\varepsilon}^r], \quad I_2 := \text{trace}[(\boldsymbol{\varepsilon} - \boldsymbol{\varepsilon}^r)^2], \quad I_4 := \text{trace}[(\boldsymbol{\varepsilon} - \boldsymbol{\varepsilon}^r)(\boldsymbol{a} \otimes \boldsymbol{a})], \\ I_5 := \text{trace}[(\boldsymbol{\varepsilon} - \boldsymbol{\varepsilon}^r)^2(\boldsymbol{a} \otimes \boldsymbol{a})], \quad J_1 := \text{trace}[(\boldsymbol{E} \otimes \boldsymbol{E})], \quad J_2 := \text{trace}[(\boldsymbol{E} \otimes \boldsymbol{a})], \\ K_1 := \text{trace}[(\boldsymbol{\varepsilon} - \boldsymbol{\varepsilon}^r)(\boldsymbol{E} \otimes \boldsymbol{a})], \quad \bar{N}^P := \text{trace}[(\boldsymbol{P}^r \otimes \boldsymbol{a})] \, . \end{gathered} \tag{23}$$

Here J_2 represents the projection of the electric field and K_1 the projection of $(\boldsymbol{\varepsilon} - \boldsymbol{\varepsilon}^r) \cdot \boldsymbol{E}$ onto the preferred direction. For a graphical interpretation of this invariants, see Fig. 4.

The enthalpy function H is formulated in terms of the elements of the polynomial basis

$$H = H(I_1, I_2, I_4, I_5, J_1, J_2, K_1, \bar{N}^P) =: H(L_i | i = 1, \ldots 8) \, , \tag{24}$$

which is invariant under all transformations $\boldsymbol{Q} \in \mathcal{O}(3)$. Of course, polynomial functions in elements of the polynomial basis are also invariant under these transformations.

4.2 Thermodynamic potential

In the framework discussed above we now construct a specific model problem. In this model the underlying thermodynamic potential is divided into five parts and given by

$$H = H_1(\boldsymbol{\varepsilon}, \boldsymbol{\varepsilon}^r) + H_2(\boldsymbol{E}) + H_3(\boldsymbol{\varepsilon}, \boldsymbol{\varepsilon}^r, \boldsymbol{E}, \bar{N}^P) + H_4(\boldsymbol{E}, \bar{N}^P) + H_5(\bar{N}^P) \, . \tag{25}$$

The first one is a pure mechanical part and therefore expressed by the basic and mixed invariants in $\boldsymbol{\varepsilon}$, $\boldsymbol{\varepsilon}^r$, and $\boldsymbol{a}$. Here we choose a quadratic function in the basic and mixed invariants associated to the mechanical strains because we are interested in a linear relation between the stresses and the reversible strains; thus we obtain

$$H_1 = \frac{1}{2}\lambda I_1^2 + \mu I_2 + \alpha_1 I_5 + \alpha_2 I_4^2 + \alpha_3 I_1 I_4 \, , \tag{26}$$

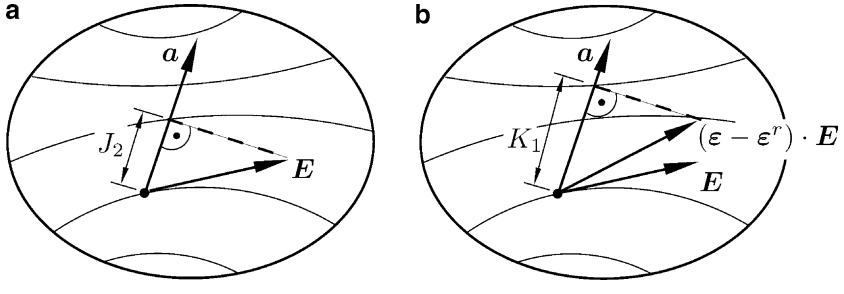

Fig. 4 Graphical interpretation of invariants **a** J_2 and **b** K_1

where the set of coefficients $\{\lambda, \mu, \alpha_1, \alpha_2, \alpha_3\}$ specifies the mechanical material properties. A pure electrical part with the corresponding material properties $\{\gamma_1, \gamma_2\}$ is given by

$$H_2 = \gamma_1 J_1 + \gamma_2 J_2^2 \ , \tag{27}$$

which represents a quadratic function in the electric field strength, in order to reflect a linear constitutive relation for the electric displacements and the electric field for the dielectric part. The coupling between the mechanical and electrical part, known as piezoelectricity, is defined by

$$H_3 = [\beta_1 I_1 J_2 + \beta_2 I_4 J_2 + \beta_3 K_1] \frac{1}{P_s} \bar{N}^P =: \omega \, \bar{N}^P \ , \tag{28}$$

with the piezoelectric material properties $\{\beta_1, \beta_2, \beta_3\}$. In order to arrive at a comprehensive notation in (28) we introduce the abbreviation ω. Here the bracketed term characterizes the linear piezoelectric response. In experiments we observe a so-called poling process in which the spontaneous polarization vectors of the unpoled specimen are more or less aligned. This process is governed by the evolution of the remanent polarization. Thus, it becomes apparent that this coupling effect is assumed to be increasing with an increasing remanent polarization until a saturation value, given by the maximum achievable polarization P_s, is reached. The terms H_4 and H_5 with

$$H_4 = -J_2 \, \bar{N}^P \quad \text{and} \quad H_5 = f(\bar{N}^P) \tag{29}$$

take into account the remanent polarization of the material, where the function $f(\bar{N}^P)$ governs the form of the dielectric hysteresis curve. This function $f(\bar{N}^P)$ is the antiderivative of a function representing the dependency between the polarization and the effective electric field. Motivated by fundamental concepts of statistical mechanics in combination with self-consistency schemes, for some remarks see e.g., [38], we choose

$$f(\bar{N}^P) = \frac{1}{c} \left[\bar{N}^P \text{Artanh} \left(\frac{\bar{N}^P}{P_s} \right) + \frac{1}{2} P_s \ln \left(1 - \left(\frac{\bar{N}^P}{P_s} \right)^2 \right) \right] \ . \tag{30}$$

Based on the constitutive expressions given in (16) the explicit form of the stresses and electric displacements appear with

$$\boldsymbol{\sigma} = \partial_{\boldsymbol{\varepsilon}} \hat{H} = \sum_{i=1}^{8} \frac{\partial \hat{H}}{\partial L_i} \frac{\partial L_i}{\partial \boldsymbol{\varepsilon}} \quad \text{and} \quad \boldsymbol{D} = -\partial_{\boldsymbol{E}} \hat{H} = -\sum_{i=1}^{8} \frac{\partial \hat{H}}{\partial L_i} \frac{\partial L_i}{\partial \boldsymbol{E}} \tag{31}$$

for the specific model problem (25) as follows:

$$\begin{aligned} \boldsymbol{\sigma} &= (\lambda I_1 + \alpha_3 I_4) \mathbf{1} + 2\mu \boldsymbol{\varepsilon} + \alpha_1 [\boldsymbol{a} \otimes \boldsymbol{\varepsilon} \boldsymbol{a} + \boldsymbol{a} \boldsymbol{\varepsilon} \otimes \boldsymbol{a}] + (2\alpha_2 I_4 + \alpha_3 I_1) \boldsymbol{a} \otimes \boldsymbol{a} \\ &\quad + [\beta_1 J_2 \mathbf{1} + \beta_2 J_2 \boldsymbol{a} \otimes \boldsymbol{a} + \frac{1}{2} \beta_3 (\boldsymbol{E} \otimes \boldsymbol{a} + \boldsymbol{a} \otimes \boldsymbol{E})] \frac{1}{P_s} \bar{N}^P \ , \\ \boldsymbol{D} &= -2\gamma_1 \boldsymbol{E} - 2\gamma_2 J_2 \boldsymbol{a} - [(\beta_1 I_1 + \beta_2 I_4) \boldsymbol{a} + \beta_3 \boldsymbol{a} \boldsymbol{\varepsilon}] \frac{1}{P_s} \bar{N}^P + \boldsymbol{P}^r \ . \end{aligned} \tag{32}$$

Here $\boldsymbol{P}^r = -\partial H_4 / \partial \boldsymbol{E} = \bar{N}^P \boldsymbol{a}$ is the remanent polarization with respect to the polarization axis. For the corresponding moduli in the linear piezoelectric range, where H_4 and H_5 are neglected and $\bar{N}^P$ is set to the maximum value of polarization P_s, we introduce the abbreviations

$$\mathbb{C} := \partial_{\boldsymbol{\varepsilon}} \boldsymbol{\sigma} \, , \quad \boldsymbol{e} := \partial_{\boldsymbol{\varepsilon}} \boldsymbol{D} = -(\partial_{\boldsymbol{E}} \boldsymbol{\sigma})^T \quad \text{and} \quad \boldsymbol{\epsilon} := \partial_{\boldsymbol{E}} \boldsymbol{D} \ . \tag{33}$$

An identification of the material parameters that are used in this coordinate-independent formulation is given in the Appendix, where the classical representation of the parameters is compared with the invariant formulation taking into account the aforementioned restrictions for the piezoelectric range.

4.3 Switching surface

The time derivative of the thermodynamic potential (25) yields

$$\begin{aligned}\dot{H} &= \partial_{\boldsymbol{\varepsilon}} H : \dot{\boldsymbol{\varepsilon}} + \partial_{\boldsymbol{\varepsilon}^r} H : \dot{\boldsymbol{\varepsilon}}^r + \partial_{\boldsymbol{E}} H \cdot \dot{\boldsymbol{E}} + \partial_{\bar{N}^P} H \cdot \dot{\bar{N}}^P \\ &= (\partial_{\boldsymbol{\varepsilon}} H_1 + \partial_{\boldsymbol{\varepsilon}} H_3) : \dot{\boldsymbol{\varepsilon}} + (\partial_{\boldsymbol{\varepsilon}^r} H_1 + \partial_{\boldsymbol{\varepsilon}^r} H_3) : \dot{\boldsymbol{\varepsilon}}^r \\ &\quad + (\partial_{\boldsymbol{E}} H_2 + \partial_{\boldsymbol{E}} H_3 + \partial_{\boldsymbol{E}} H_4) \cdot \dot{\boldsymbol{E}} + (\partial_{\bar{N}^P} H_3 + \partial_{\bar{N}^P} H_4 + \partial_{\bar{N}^P} H_5) \cdot \dot{\bar{N}}^P \ ,\end{aligned} \tag{34}$$

and the evaluation of the second law of thermodynamics leads, for the specific model problem (25) with (32), to the reduced dissipation inequality

$$\underbrace{-(\partial_{\boldsymbol{\varepsilon}^r} H_1 + \partial_{\boldsymbol{\varepsilon}^r} H_3)}_{\tilde{\boldsymbol{\sigma}}} : \dot{\boldsymbol{\varepsilon}}^r \ \underbrace{-(\partial_{\bar{N}^P} H_3 + \partial_{\bar{N}^P} H_4 + \partial_{\bar{N}^P} H_5)}_{\tilde{E}} \cdot \dot{\bar{N}}^P \geq 0 \ . \tag{35}$$

We recast this formulation according to (17) in $\tilde{\boldsymbol{\sigma}} : \dot{\boldsymbol{\varepsilon}}^r + \tilde{E} \cdot \dot{\bar{N}}^P \geq 0$. Following [28] we use the constitutive relation

$$\boldsymbol{\varepsilon}^r = \frac{\varepsilon_a^r}{P_s^2} \operatorname{dev}(\boldsymbol{P}^r \otimes \boldsymbol{P}^r) \ , \tag{36}$$

where ε_a^r characterizes the maximum achievable remanent strain due to polarization in the direction of the polarization axis. This quadratic relationship between the remanent polarization and strains is a commonly reasonable assumption, when the electric fields are strong and the stresses are small, see e.g., [16]. Thus, the reduced dissipation inequality appears in the form

$$\tilde{E} \cdot \dot{\bar{N}}^P \geq 0 \ , \tag{37}$$

and the remaining evolution equation for the internal variable $\bar{N}^P$, following the outline in Sect. 3.2, is

$$\dot{\bar{N}}^P = \lambda \partial_{\tilde{E}} \phi = \lambda \tilde{n} \ . \tag{38}$$

As a simple choice for the switching criterion we specify

$$\Phi = \tilde{E}^2 - E_c^2 \leq 0 \ , \tag{39}$$

with the coercive field strength E_c. The quantity $\tilde{E}$ is decomposed into $\tilde{E} = E - E^B$, with

$$E := -\partial_{\bar{N}^P} H_4 = J_2 \quad \text{and} \quad E^B := \partial_{\bar{N}^P} H_3 + \partial_{\bar{N}^P} H_5 \ , \tag{40}$$

the projection of the electric field in the preferred direction and the so-called back electric field, respectively. Now the switching criterion appears in the explicit form

$$\Phi = (E - E^B)^2 - E_c^2 = (J_2 - E^B)^2 - E_c^2 \leq 0 \ . \tag{41}$$

Let us now consider a typical time interval $[t_n, t_{n+1}]$ and denote the quantities $(\bullet)$ at time t_{n+1} with $(\bullet)_{n+1}$ and at time t_n with $(\bullet)_n$. Due to the given variational formulation of the finite element in the basic quantities $\boldsymbol{E}$ (and $\boldsymbol{\varepsilon}$), $J_{2,n+1}$ is fixed in the actual iteration step. Thus, for the loading case $\Phi = 0$, (41) can be solved with respect to the back electric field, i.e.

$$\begin{aligned} E^B_{n+1} &= J_{2,n+1} + E_c \quad \text{if} \quad J_{2,n+1} < J_{2,n} \\ E^B_{n+1} &= J_{2,n+1} - E_c \quad \text{otherwise} \ . \end{aligned} \tag{42}$$

Taking into account the definition of E^B given in (40) and the entering terms (25)–(30), we obtain an implicit function for the projection of the remanent polarization in the preferred direction

$$E^B_{n+1} = \omega + f'\left(\bar{N}^P_{n+1}\right) \quad \text{with} \quad f'(\bar{N}^P_{n+1}) = \frac{1}{c} \operatorname{Artanh}\left(\frac{\bar{N}^P_{n+1}}{P_s}\right) \ . \tag{43}$$

Applying a backward Euler approximation scheme to the evolution Eq. (38) yields the update formula

$$\bar{N}^P_{n+1} = \bar{N}^P_n + \Delta\lambda \tilde{n}_{n+1} \quad \text{with} \quad \Delta\lambda := \Delta t \ \lambda \tag{44}$$

and $\Delta t = t_{n+1} - t_n$. The unknown parameter $\Delta\lambda$ can be obtained by solving $(43)_1$, where the left-hand side is given by (42). This straightforward procedure for the calculation of the remanent polarization $\bar{N}^P$ results from the fact that the switching criterion is formulated in the basic variable $\boldsymbol{E} := -\operatorname{grad}[\phi]$ of the finite-element approximation.

5 Numerical examples

5.1 Homogeneous bar

In this example we point out the characteristic hysteresis loops for a ferroelectric crystal. We consider a simply supported bar of length $l = 2\,\text{mm}$ and height $h = 1\,\text{mm}$ that is discretized with two four-node standard displacement/electric potential elements. At the left edge the electric potential is set to zero, whereas a time-varying electric potential $\phi(t)$ at the right edge is prescribed. In Fig. 5a the system with the corresponding boundary conditions and the relative distribution of the electric potential is given for $\phi(t) \neq 0$. Figure 5b depicts the variation of the electric field versus time.

The material parameters used in this example are chosen in accordance with that found in [16] for single-crystal barium titanate. The material parameters for the elastic stiffness tensor are set to

$$\mathbb{C}_{11} = 166\,, \quad \mathbb{C}_{12} = 76.6\,, \quad \mathbb{C}_{13} = 77.5\,, \quad \mathbb{C}_{33} = 162\,, \quad \mathbb{C}_{44} = 42.9 \tag{45}$$

in units of $10^3\,\text{N/mm}^2$. The components of the piezoelectric tensor are chosen to be

$$e_{31} = -4.4\,, \quad e_{33} = 18.6\,, \quad e_{15} = 11.6 \tag{46}$$

in units of $10^{-3}\,\text{N/Vmm}$. The parameters for the dielectric tensor are set to

$$\kappa_{11} = 1260 \cdot \epsilon_0 = 1.12\,, \quad \kappa_{33} = 1420 \cdot \epsilon_0 = 1.26 \tag{47}$$

in units of $10^{-11}\,\text{C/Vmm}$, where $\epsilon_0 = 8.854 \times 10^{-15}\text{C/Vmm}$ is the permittivity of free space. The conversion of the elastic (45), piezoelectric (46), and dielectric (47) parameters into those used for the coordinate-invariant formulation are given in the Appendix. At a temperature of approximately 25°C one can find the following corresponding values for the maximum achievable polarization P_s and the coercive field E_c:

$$P_s = 26 \times 10^{-8}\text{C/mm}^2\,; \quad E_c = 1000\,\text{V/mm}\,. \tag{48}$$

For the maximum remanent strain along the polarization direction that is introduced in (36) we choose $\varepsilon_a^r = 0.001$, where the preferred direction $\boldsymbol{a}$ points along the center line of the bar from the fixed to the mobile boundary. Once the switching criterion (39) is identically fulfilled, i.e. the coercive field E_c is reached and therefore $\Phi = 0$, the evolution of the remanent quantities $\boldsymbol{P}^r$ and $\boldsymbol{\varepsilon}^r$ is initiated, controlled by function (30). The maximum value of the remanent polarization is P_s, and the slope of the hysteresis curves is governed by the parameter c. The calculated hysteresis loops for a simply supported bar under a cyclic varying electric field, see Fig. 5, are given in Fig. 6, for different parameters c. It is observable that, with an increasing parameter c, the hysteresis loops are similar to hysteresis loops exhibited by an ideal crystal, see e.g., [38].

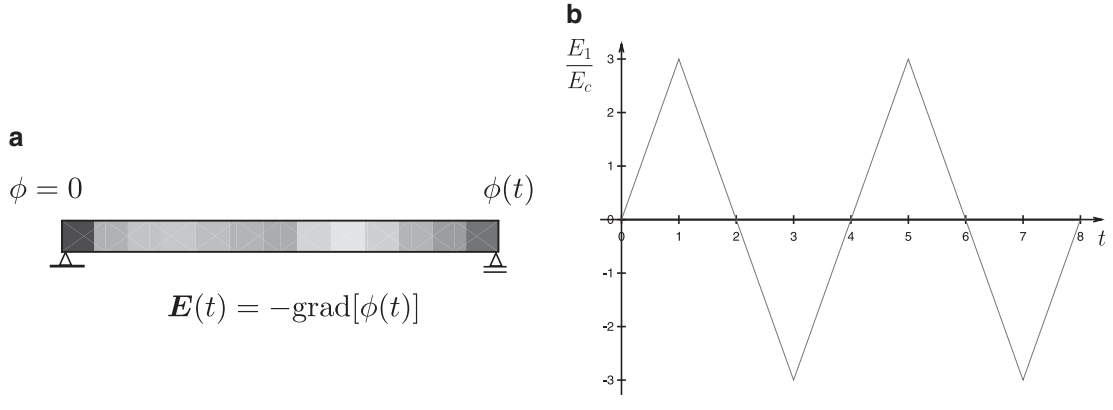

Fig. 5 **a** Boundary conditions and relative distribution of the electric potential, and **b** variation of electric field versus time

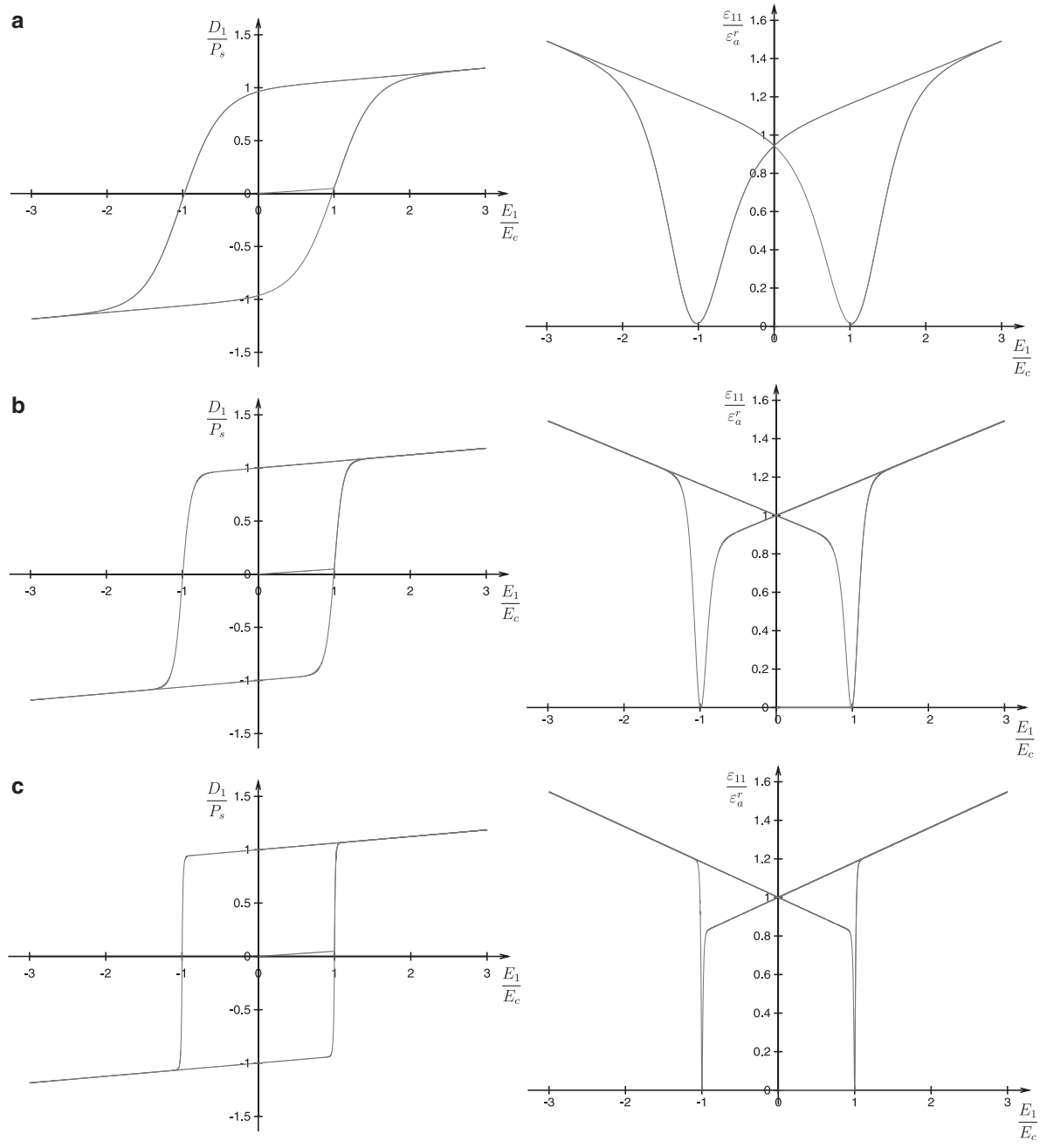

Fig. 6 Hysteresis curves for **a** $c = 0.002$, **b** $c = 0.008$, and **c** $c = 0.04$

5.2 Square plate with a notch

In the following example we consider a square plate, with dimensions of 20×20 mm and a centered notch, length 12 mm and a maximum height of 0.4 mm in the middle. Due to the symmetry of the plate, only a quarter of the specimen is discretized with 1960 four-node standard displacement/electric potential elements. The unreleased regions of the right and lower edge of the specimen are fixed in an upright direction to the corresponding edge, whereas at the lower edge the electric potential is additionally set to zero, see Fig. 7. At the upper edge we prescribe a time-varying electric potential $\phi(t)$ similar to the loading depicted in Fig. 5b. For the maximum value of $\phi(t = 1\,\mathrm{s}) = -\phi(t = 3\,\mathrm{s})$ we choose -100 kV. The vector $\boldsymbol{a}$ points in the vertical direction and the parameter c is set to 0.0002. For the mechanical, dielectric, and piezoelectric material parameters as

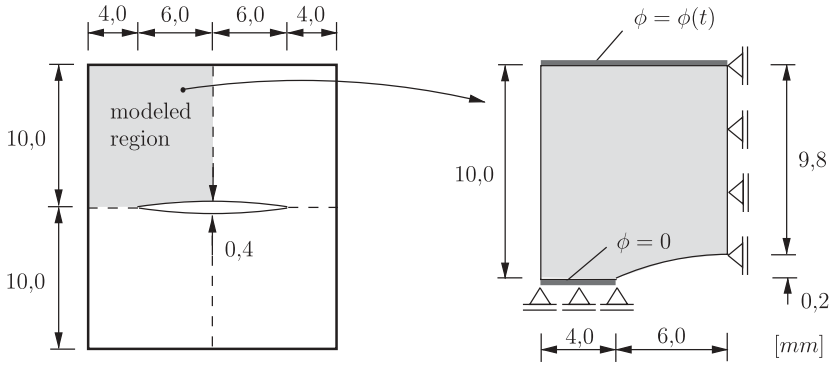

Fig. 7 Square plate with a notch, geometry and boundary conditions

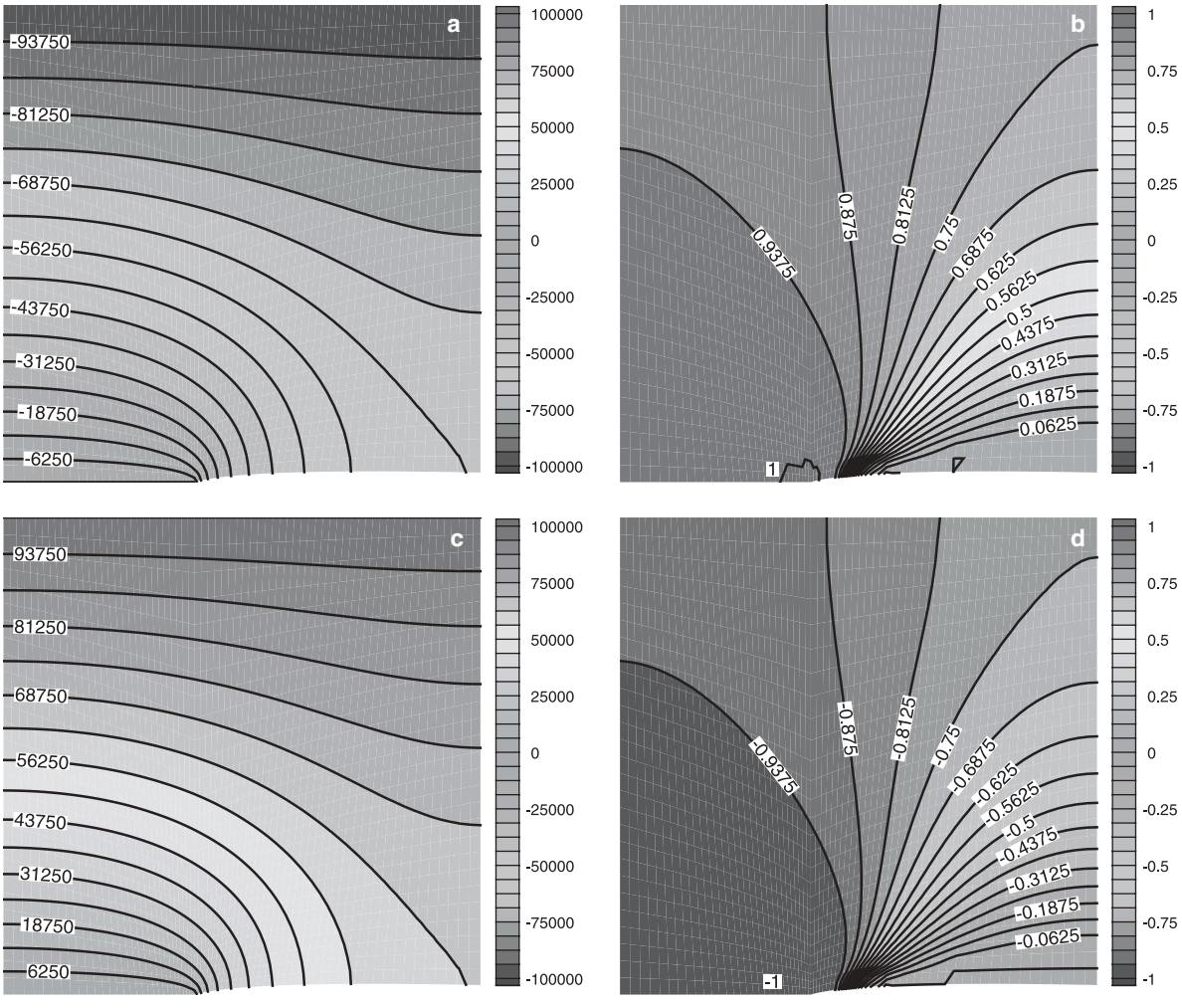

Fig. 8 Distribution of $\phi(t)$ for **a** $t = 1.0\,\mathrm{s}$ and **c** $t = 3.0\,\mathrm{s}$. Distribution of $\boldsymbol{P}^r \cdot \boldsymbol{a}/P_s$ for **b** $t = 1.0\,\mathrm{s}$ and **d** $t = 3.0\,\mathrm{s}$

well as for the saturation value of polarization and the coercive field strength, we choose the same values as in the first example. The distribution of ϕ and the associated normalized values of the remanent polarization in the preferred direction are depicted in Fig. 8 for $t = 1\,\mathrm{s}$ and $t = 3\,\mathrm{s}$, respectively.

6 Conclusions

We have proposed a fully electromechanical coupled formulation for an assumed transversely isotropic ceramic suitable for the modeling of the characteristic dielectric and butterfly hysteresis loops. Based on tensor representation theorems and applying the concept of isotropy of space, the thermodynamic potential acts as an isotropic tensor function. This has been formulated in terms of basic and mixed invariants of the total strains, remanent strains, electric field, remanent polarization, and a first-order structural tensor. In this coordinate-invariant setting the constitutive laws fulfill automatically the material symmetry requirements of the anisotropic material. Evaluating the second law of thermodynamics leads to constitutive expressions for the stresses and electric displacements. Furthermore, the reduced dissipation inequality is enforced by the assumed switching surface, which yields, applying the postulate of maximum remanent dissipation, associated flow rules for the remanent quantities. For the remanent strains we have chosen the often-used constitutive assumption—in the case of strong electric fields and small stresses—that this quantity is proportional to the deviatoric part of the dyadic product of the remanent polarization. The evolution of the remanent polarization is governed by a quadratic switching surface, and the slope of the hysteresis curves are described by an implicit function. The underlying computational framework allows a straightforward (simple) calculation of the remanent polarization vector because the basic electrical field quantity of the finite-element approximation and that entering the switching surface are the same.

A Identification of material parameters

The classical constitutive equations for the stress tensor $\boldsymbol{\sigma}$ and the electric displacement field $\boldsymbol{D}$ of a piezoelectric solid are given by

$$\boldsymbol{\sigma} = \mathbb{C} : \boldsymbol{\varepsilon} - \boldsymbol{e}^T \cdot \boldsymbol{E} \quad \text{and} \quad \boldsymbol{D} = \boldsymbol{e} : \boldsymbol{\varepsilon} + \boldsymbol{\epsilon} \cdot \boldsymbol{E} \,, \tag{49}$$

see, e.g. [30]. Here $\mathbb{C}$ denotes the fourth-order elasticity tensor, $\boldsymbol{e}$ the third-order tensor of piezoelectric moduli, and $\boldsymbol{\epsilon}$ the second-order tensor of dielectric moduli. In the considered case of transverse isotropy there exist five elastic constants, three piezoelectric constants, and two dielectric constants, due to the restrictions on the linearly independent constants, induced by the symmetry group. If the preferred direction $\boldsymbol{a}$ coincides with the x_3-axis, the coordinate-dependent representation of the mechanical moduli in the case of transverse isotropy is given by

$$\mathbb{C} = \begin{bmatrix} \mathbb{C}_{11} & \mathbb{C}_{12} & \mathbb{C}_{13} & 0 & 0 & 0 \\ \mathbb{C}_{12} & \mathbb{C}_{11} & \mathbb{C}_{13} & 0 & 0 & 0 \\ \mathbb{C}_{13} & \mathbb{C}_{13} & \mathbb{C}_{33} & 0 & 0 & 0 \\ 0 & 0 & 0 & \frac{1}{2}(\mathbb{C}_{11} - \mathbb{C}_{12}) & 0 & 0 \\ 0 & 0 & 0 & 0 & \mathbb{C}_{44} & 0 \\ 0 & 0 & 0 & 0 & 0 & \mathbb{C}_{44} \end{bmatrix} , \tag{50}$$

with five independent constants. The matrix notation follows from the index arrangement for the stresses $\boldsymbol{\sigma} := (\sigma_{11}, \sigma_{22}, \sigma_{33}, \sigma_{12}, \sigma_{23}, \sigma_{13})^T$ and the arrangement for the strains $\boldsymbol{\varepsilon} := (\varepsilon_{11}, \varepsilon_{22}, \varepsilon_{33}, 2\varepsilon_{12}, 2\varepsilon_{23}, 2\varepsilon_{13})^T$. Furthermore, the matrix representation for the piezoelectric and dielectric constants yields

$$\boldsymbol{e} = \begin{bmatrix} 0 & 0 & 0 & 0 & 0 & e_{15} \\ 0 & 0 & 0 & 0 & e_{15} & 0 \\ e_{31} & e_{31} & e_{33} & 0 & 0 & 0 \end{bmatrix} \quad \text{and} \quad \boldsymbol{\epsilon} = \begin{bmatrix} \epsilon_{11} & 0 & 0 \\ 0 & \epsilon_{11} & 0 \\ 0 & 0 & \epsilon_{33} \end{bmatrix} , \tag{51}$$

with three independent piezoelectric and two independent dielectric constants. A comparison of the parameters used for the invariant formulation (32) with the coordinate-dependent formulation given above leads for the mechanical properties to

$$\begin{aligned} \lambda = \mathbb{C}_{12} \,, \quad \mu = \tfrac{1}{2}(\mathbb{C}_{11} - \mathbb{C}_{12}) \,, \quad \alpha_1 = 2\mathbb{C}_{44} + \mathbb{C}_{12} - \mathbb{C}_{11} \,, \\ \alpha_2 = \tfrac{1}{2}(\mathbb{C}_{11} + \mathbb{C}_{33}) - 2\mathbb{C}_{44} - \mathbb{C}_{13} \,, \quad \alpha_3 = \mathbb{C}_{13} - \mathbb{C}_{12} \,, \end{aligned} \tag{52}$$

for the piezoelectric properties to

$$\beta_1 = -e_{31} \,, \quad \beta_2 = -e_{33} + 2e_{15} + e_{31} \,, \quad \beta_3 = -2e_{15} \tag{53}$$

and for the dielectric properties to

$$\gamma_1 = -\epsilon_{11}/2 \,, \quad \gamma_2 = \tfrac{1}{2}(\epsilon_{11} - \epsilon_{33}) \,. \tag{54}$$

For more details we refer the reader to [31].

References

1. Bassiouny, E., Ghaleb, A.F., Maugin, G.A.: Thermodynamical formulation for coupled electromechanical hysteresis effects. I. Basic equations. Int J Eng Sci **26**, 1279–1295 (1988)
2. Bassiouny, E., Ghaleb, A.F., Maugin, G.A.: Thermodynamical formulation for coupled electromechanical hysteresis effects. II. Poling of ceramics. Int J Eng Sci **26**, 1297–1306 (1988)
3. Bassiouny, E., Maugin, G.A.: Thermodynamical formulation for coupled electromechanical hysteresis effects. III. Parameter identification. Int J Eng Sci **27**, 975–987 (1989)
4. Bassiouny, E., Maugin, G.A.: Thermodynamical formulation for coupled electromechanical hysteresis effects. IV. Combined electromechanical loading. Int J Eng Sci **27**, 989–1000 (1989)
5. Boehler, J.P.: Introduction to the invariant formulation of anisotropic constitutive equations. In: Boehler, J.P. (ed.) Applications of tensor functions in solid mechanics. CISM Course no. 292. Springer, Berlin Heidelberg New York (1987)
6. Boehler, J.P.: Representations for isotropic and anisotropic non-polynominal tensor functions. In: Boehler, J.P. (ed.) Applications of Tensor Functions in Solid Mechanics. CISM Course no. 292. Springer, Berlin Heidelberg New York (1987)
7. Chen, P.J., Montgomery, S.T.: A macroscopic theory for the existence of the hysteresis and butterfly loops in ferroelectricity. Ferroelectrics **23**, 199–208 (1980)
8. Chen, P.J., Tucker, T.J.: One dimensional polar mechanical and dielectric responses of the ferroelectric ceramic PZT 65/35 due to domain switching. Int J Eng Sci **19**, 147–158 (1981)
9. Cocks, A.C.F., McMeeking, R.M.: A phenomenological constitutive law for the behavior of ferroelectric ceramics. Ferroelectrics **228**, 219–228 (1999)
10. Eringen, A.C., Maugin, G.A.: Electrodynamics of Continua. Vol. **1**, Foundations and Solid Media. Springer, Berlin Heidelberg New York (1990)
11. Eringen, A.C., Maugin, G.A.: Electrodynamics of Continua. Vol. **2**, Fluid and Complex Media. Springer, Berlin Heidelberg New York (1990)
12. Hwang, S.C., Lynch, C.S., McMeeking, R.M.: Ferroelectric/ferroelastic interactions and a polarization switching model. Acta Metallurg Material **43**, 2073–2084 (1995)
13. Hwang, S.C., McMeeking R.: The prediction of switching in polycrystalline ferroelectric ceramics. Ferroelectrics **207**, 465–495 (1998)
14. Hwang, S.C., McMeeking R.: A finite element model of ferroelectric polycrystals. Ferroelectrics **211**, 177–194 (1998)
15. Hwang, S.C., McMeeking R.: A finite element model of ferroelastic polycrystals. Int J Solids Struct **36**, 1541–1556 (1999)
16. Jaffe, B., Cook, W.R., Jaffe, H.: Piezoelectric Ceramics. Academic, London (1971)
17. Kamlah, M., Tsakmakis, C.: Phenomenological modelling of the non-linear electro-mechanical coupling in ferroelectrics. Int J Solids Struct **36**, 669–695 (1999)
18. Kamlah, M., Böhle, U.: Finite element analysis of piezoceramic components taking into account ferroelectric hysteresis behavior. Int J Solids Struct **38**, 605–633 (2001)
19. Kamlah, M.: Ferroelectric and ferroelastic piezoceramics—modeling of electromechanical hysteresis phenomena. Continuum Mech Thermodyn **13**, 219–268 (2001)
20. Kamlah, M., Wang, Z.: A thermodynamically and microscopically motivated constitutive model for piezoceramics. Comput Mat Sci **28**, 409–418 (2003)
21. Landis, C.M.: Fully coupled, multi-axial, symmetric constitutive laws for polycrystalline ferroelectric ceramics. J Mech Phys Solids **50**, 127–152 (2002)
22. Landis, C.M.: A new finite-element formulation for electromechanical boundary value problems. Int J Numer Methods Eng **55**, 613–628 (2002)
23. Lemaitre, J., Chaboche J.-L.: Mechanics of solid materials. Cambridge University Press, Cambridge (1990)
24. Liu, I-Shih: On representations of anisotropic invariants. Int J Eng Sci **20**, 1099–1109 (1982)
25. Luenberger, D.G.: Linear and nonlinear programming. Addison-Wesley, Reading, MA (1984)
26. Lupascu, D.C., Rödel, J.: Fatigue in bulk lead zirconate actuator materials: a review. Report des Institutes Nictqtmetalliscq-Auorganiscqe Werkstoffe der TV-Darmstadt (2004)
27. Lynch, C.S.: On the development of multiaxial phenomenological constitutive laws for ferroelectric ceramics. J Intell Mat Syst Struct **9**, 555–563 (1998)
28. McMeeking, R.M., Landis, C.M.: A phenomenological multi-axial constitutive law for switching in polycrystalline ferroelectric ceramics. Int J Eng Sci **40**, 1553–1577 (2002)
29. Mielke, A., Timofte, A.M.: An energetic material model for time-dependent ferroelectric behavior: existence and uniqueness. WIAS Preprint No. 1014 (2005)
30. Nowacki, W.: Foundations of linear piezoelectricity. In: Parkus, H. (ed.) Electromagnetic Interactions in Elastic Solids. CISM course no. 257. Springer, Berlin Heidelberg New York (1979)

31. Schröder, J., Gross, D.: Invariant formulation of the electromechanical enthalpy function of transversely isotropic piezoelectric materials. Arch Appl Mech **73**, 533–552 (2004)
32. Smith, G.F.: On a fundamental error in two papers of C.C. Wang. Arch Rat Mech Anal **36**, 161–165 (1970)
33. Smith, G.F.: On isotropic functions of symmetric tensors, skew-symmetric tensors and vectors. Int J Eng Sci **19**, 899–916 (1971)
34. Spencer, A.J.M.: Theory of invariants. In: Eringen, A.C. (ed.) Continuum Physics, Vol. **1**. Academic, New York (1971)
35. Spencer, A.J.M.: Isotropic polynomial invariants and tensor functions. In: Boehler, J.P. (ed.) Applications of Tensor Functions in Solid Mechanics. CISM course no. 282. Springer, Berlin Heidelberg New York (1987)
36. Wang, C.C.: On representations for isotropic functions: Part I. Isotropic functions of symmetric tensors and vectors. Arch Rat Mech Anal **33**, 249–267 (1969)
37. Wang, C.C.: On representations for isotropic functions: Part II. Isotropic functions of skew-symmetric tensors, symmetric tensors and vectors. Arch Rat Mech Anal **33**, 268–287 (1969)
38. Zheludev, I.S.: Physics of Polycrystalline Dielectrics. Vol. **2**, Electrical Properties. Plenum, New York (1971)